Journal of Photochemistry and Photobiology A: Chemistry 220 (2011) 188–194

Contents lists available at ScienceDirect

Journal of Photochemistry and Photobiology A: Chemistry

journal homepage: www.elsevier.com/locate/jphotochem

UV laser photodeposition of nanomagnetic soot from gaseous benzene and acetonitrile–benzene mixture

Josef Pola[a,*], Akihiko Ouchi[b,**], M. Maryško[c], V. Vorlíček[c], Jan Šubrt[d], S. Bakardjieva[d], Zdeněk Bastl[e]

[a] Laboratory of Laser Chemistry, Institute of Chemical Process Fundamentals, ASCR, 16502 Prague, Czech Republic
[b] National Institute of Advanced Industrial Science and Technology, AIST Tsukuba, Ibaraki 305-8565, Japan
[c] Institute of Physics, ASCR, 18223 Prague 8, Czech Republic
[d] Institute of Inorganic Chemistry, ASCR, 25068 Řež, Czech Republic
[e] J. Heyrovský Institute of Physical Chemistry, ASCR, 18223 Prague, Czech Republic

ARTICLE INFO

Article history:
Received 22 January 2011
Received in revised form 29 March 2011
Accepted 2 April 2011
Available online 12 April 2011

Keywords:
Benzene
Acetonitrile
Laser photodeposition
Nanomagnetic soot
CN-substituted soot

ABSTRACT

Megawatt KrF laser gas-phase photolysis of benzene and acetonitrile–benzene mixture was studied by using mass spectroscopy–gas-chromatography and Fourier transform infrared spectroscopy for analyses of volatile products, and by Fourier transform infrared, Raman and X-ray photoelectron spectroscopy, electron microscopy and magnetization measurements for analyses of solid products deposited from the gas-phase. The results are consistent with carbonization of benzene and decomposition of non-absorbing acetonitrile in carbonizing benzene through collisions with excited benzene and/or its fragments. The solid products from benzene and acetonitrile–benzene mixture have large surface area and are characterized as nanomagnetic amorphous carbonaceous soot containing unsaturated C centers prone to oxidation. The nanosoot from acetonitrile–benzene mixture incorporates CN groups, confirms reactions of benzene fragments with CN radical and has a potential for modification by reactions at the CN bonds.

1. Introduction

UV laser irradiation of gaseous benzene has been broadly studied with the aim to identify the decomposition mechanism and products. Early experiments revealed isomers (benzvalene, fulvene and 1,3-hexadiene-5-yne), fragmentation products (methane, ethane, ethane, ethyne) and a carbonaceous solid deposited on the cell walls (e.g. [1–3]).

Later experiments under collisionless conditions using ArF and KrF lasers have shown that primary photodissociation channels is cleavage of the C–H bond and all possible fissions of benzene carbon ring (namely $C_6H_5 + H$, $C_6H_4 + H_2$, $C_5H_3 + CH_3$, and $C_4H_3 + C_2H_3$ [4–6]). These steps were confirmed by ab initio RRKM study [7]. Other reactions were recognized in UV laser collisionless conditions by using a CARS (coherent anti-Stokes Raman scattering) and optical and mass spectral probe techniques. These are two-photon ArF laser-induced formation of 1,3-hexadiene-5-yne and phenyl radical [8], multiphoton induced formation of C_2 fragments [9] and multiphoton ionization of benzene to a multitude of C_n/H_m ions [10–12].

Studies on UV laser gas-phase photolysis of benzene in collisional conditions are limited for KrF laser-induced formation of benzene clusters [13] and aerosol (biphenyl and phenylcyclohexadiene) photocondensation [14].

No UV laser photolytic deposition of carbon materials from benzene have yet been reported, in spite of benzene use as a precursor for carbon films and powders in plasma-assisted and laser-pyrolytic degradations.

Here we report on KrF laser-induced photolysis of benzene in the absence and presence of non-absorbing acetonitrile for gas-phase deposition of ultrafine carbonaceous powders (soot). We identify volatile and solid products of both photolyses, reveal incorporation of –CN substituents in soot produced from acetonitrile–benzene mixture and establish magnetism in both types of soot.

2. Experimental

Laser irradiation experiments were carried out on gaseous benzene (50 Torr) and a benzene (50–Torr)–acetonitrile (20 Torr) mixture in helium (total pressure 760 Torr) admitted to a previously described reactor [15]. The reactor (140 ml in volume) had two orthogonally positioned tubes: one furnished with UV-grade synthetic silica and the other with KBr windows. It possessed two side arms: one fitted with a rubber septum and the other connecting to a standard vacuum manifold. The LPX 210i KrF laser used

* Corresponding author. Tel.: +420 2 20390308; fax: +420 2 20920661.
** Corresponding author. Tel.: +8129 861 4550; fax: +8129 861 4421.
E-mail addresses: pola@icpf.cas.cz (J. Pola), ouchi.akihiko@aist.go.jp (A. Ouchi).

1010-6030/$ – see front matter © 2011 Elsevier B.V. All rights reserved.
doi:10.1016/j.jphotochem.2011.04.011

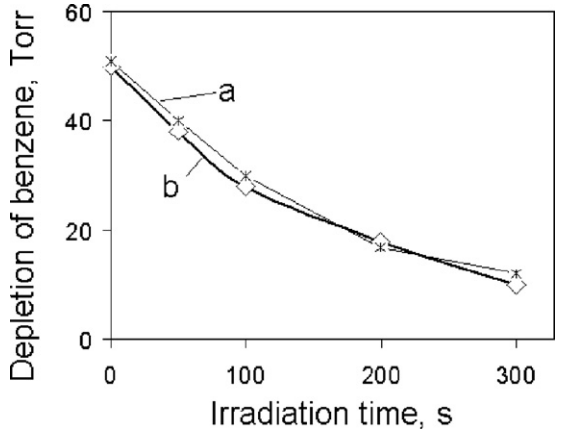

Fig. 1. Photolysis progress in benzene (a) and acetonitrile–benzene mixture (b).

for the irradiation was operated with a repetition frequency of 10 Hz at 248 nm. The pulses (580 mJ) were focused to an incident area of ca. 0.20 cm^2 and corresponded to ~25 MW (megawatt) output and 125 MW cm^2 incident intensity. They represented critical threshold, since the described sooting does not take place at lower values.

The progress of benzene photolysis was monitored directly in the reactor by Fourier Transform Infrared (FTIR) spectroscopy (a Shimadzu FTIR IR Prestige-21 spectrometer) using diagnostic absorption band at 3046 cm^{-1}. (Similar monitoring of acetonitrile was hampered by a low infrared absorption of this compound.) The irradiated reactor content was analyzed by gas-chromatography–mass spectroscopy (a Shimadzu QP 5050 mass spectrometer, 60 m capillary column Neutrabond-1, programmed temperature 30–200 °C). The decomposition products were identified through their FTIR diagnostic bands (ethyne, 730 cm^{-1}; butadiyne, 628 cm^{-1}) and through mass spectra using the NIST library.

The samples of the deposited ultrafine soot were analyzed by X-ray photoelectron (XPS), FTIR and Raman spectroscopies and by electron microscopy and were also diagnosed for physical absorption and examined for magnetic properties.

The C1s, N1s and O1s photoelectron and C KLL Auger electron spectra of the deposit were measured by using an ESCA 310 (Scienta) electron spectrometer with a base pressure better than 10^{-9} Torr and Al Kα radiation (1486.6 eV) for electron excitation. The surface composition of the deposited film was determined by correcting the spectral intensities for subshell photoionization cross-sections.

The Raman spectra were recorded on a Renishaw (a Ramascope model 1000) Raman microscope with a CCD detector using the exciting beam of an Ar-ion laser (514.5 nm, 50 mW). The beam was attenuated to obtain incident energy densities lower than 5×10^{-3} W/cm^2.

The FTIR spectra of thin layers of the deposited soot accommodated between KBr plates were obtained on a Nicolet Impact 400 spectrometer.

The SEM (Scanning Electron Microscopy) analyses were conducted on a Philips XL 30 CP scanning electron microscope equipped with energy dispersive analyzer (EDAX DX-4) of X-ray radiation. A PV 9760/77 detector in low vacuum mode (0.5 Torr) was used for quantitative determination of C, O and N elements.

The transmission electron micrographs (TEM) were obtained using a JEOL JEM 3010 microscope (LaB6 cathode) operating at 300 kV and equipped with EDS detector (INCA/Oxford) and CCD Gatan (Digital Micrograph software). The samples were prepared by grinding and subsequently dispersing the powder in ethanol and applying a drop of very dilute suspension on Ni grid.

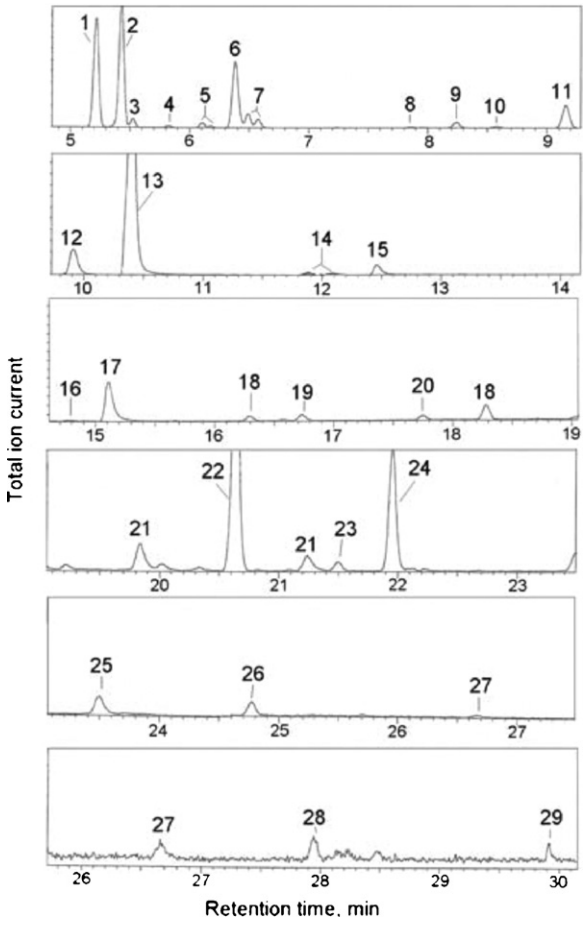

Fig. 2. GC/MS trace of volatile products in KrF laser photolysis of benzene–acetonitrile mixture. (Peak designation: 1, CO; 2, ethyne; 3, propane; 4, *cyanogen*; 5, propene; 6, *hydrogen cyanide*; 7, C_3H_4 (propyne and allene); 8, 1,3-butadiene; 9, 1-buten-3-yne; 10, 1-butyne; 11, 1,3-butadiyne; 12, *propiolonitrile*; 13, acetonitrile; 14, C_5H_6; 15, *2-propenenitrile*; 16, 3-penten-1-yne; 17, *propanenitrile*; 18, C_5H_4; 19, *2-methylpropenenitrile*; 20, *2-methylpropanenitrile*; 21, *1-cyanoprop-1-yne* or *cyanoallene*; 22, benzene; 23, hex-3-en-1,5-diyne; 24, hexa-1,3,5-triyne; 25, *pyridine*; 26, toluene; 27, $C_4N_2H_2$ (*methylenepropanedinitrile* and/or *2-butanedinitrile*); 28, ethynylbenzene; 29, benzonitrile. (CN-containing products are given in italics).

The magnetic measurements were performed in the temperature region 5–300 K using a SQUID (Superconducting Quantum Interference Device) magnetometer MPMS-5S. Deposited carbon soot was treated with a mixture of sulfuric and nitric acid and then elemental analyses for Fe, Co Mn and Ni were carried out by atomic absorption spectroscopy (Avanta Σ, GBS) and showed these impurities less than 20 ppm.

Benzene (Wako, purity 99.9%) and acetonitrile (Cica reagent, purity 99.7%) were distilled prior to use.

3. Results and discussion

3.1. Laser photolysis

KrF laser photolysis of gaseous benzene (50 Torr in He) carried out for 5 min results in 80% decomposition of benzene (Fig. 1), formation of a multitude of gaseous products (CO, ethyne, propene, allene, propyne, 1-buten-3-yne, 1-butyne, 1,3-butadiene, 1,3-butadiyne, penten-1-yne, C_5H_4, hex-3-en-1,5-diyne, 24, hexa-1,3,5-triyne, toluene and phenylacetylene) and deposition of a dark

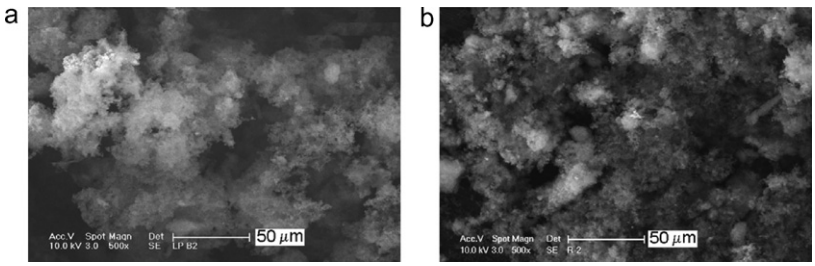

Fig. 3. SEM image of soot deposited from benzene (a) and benzene–acetonitrile mixture (b).

ultrafine carbon soot. The formation of CO proves the occurrence of minor carbothermal reaction between carbon fragments and silica reactor window [15]. The highly unsaturated C_1–C_8 hydrocarbons document a number of cleavage and combination reactions of C/H fragments, which occur in collisional regime and finally lead to the deposited carbonaceous solid. We estimate that the volatile hydrocarbons are formed in amounts lower than 10% of the depleted benzene, which is compatible with benzene mostly consumed for deposition of the dark soot.

Ethyne (the main product) and other C_3–C_6 unsaturated hydrocarbons (particularly 1,3-butadiyne and hexa-1,3,5-triyne) indicate that carbonization takes place primarily through agglomerization of small C_n (mostly C_{2n}) species [7,15–17] and not through intermediary polyaromatic hydrocarbons [18]. The observed hydrocarbons are in keeping with dehydrogenation steps, cleavage of C_6 ring to ethyne and ethynyl radical, isomerization of ethyne to ethylidene [19], radical recombination and H-abstraction and attack onto the π-electron density of the intermediates [20]. The presence of ethynylbenzene suggests this molecule as a source of cyclic carbonaceous structures.

KrF laser photolysis of benzene (50 Torr)–acetonitrile (20 Torr) in He shows similar progress as the photolysis of benzene (Fig. 1) and leads to hydrocarbons whose pattern is almost the same as that observed in photolysis of benzene alone. In this case, however, the hydrocarbons are accompanied not only with CO and a dark soot, but also with many CN-substituted volatile compounds (Fig. 2). The CN-containing products are HCN (the main product), cyanogen (NC–CN), three-carbon molecules (HC≡C–CN, H_2C=CH–CN, C_2H_5–CN), four-carbon molecules (H_2C=C(CH_3)CH_2–CN, $CH_3CH(CH_3)CH_2CN$, CH_3C≡C–CN, CH_2=C=CH–CN, $(CN)_2C$=CH_2, CN–HC=CH–CN) and benzonitrile.

In discussing formation of these CN-substituted products, we note that acetonitrile is transparent above 190 nm and that the 248 nm irradiation of CH_3CN (20 Torr in He) for 5 min does not lead to any decomposition. The CN-containing products therefore indicate that CH_3CN molecules decompose thermally in the sooting environment of photolyzed benzene through collisions with hot C/H molecules and fragments. Such thermal decomposition of CH_3CN may take place via H atom ejection and involvement of open shell products which are, in the decreasing importance,

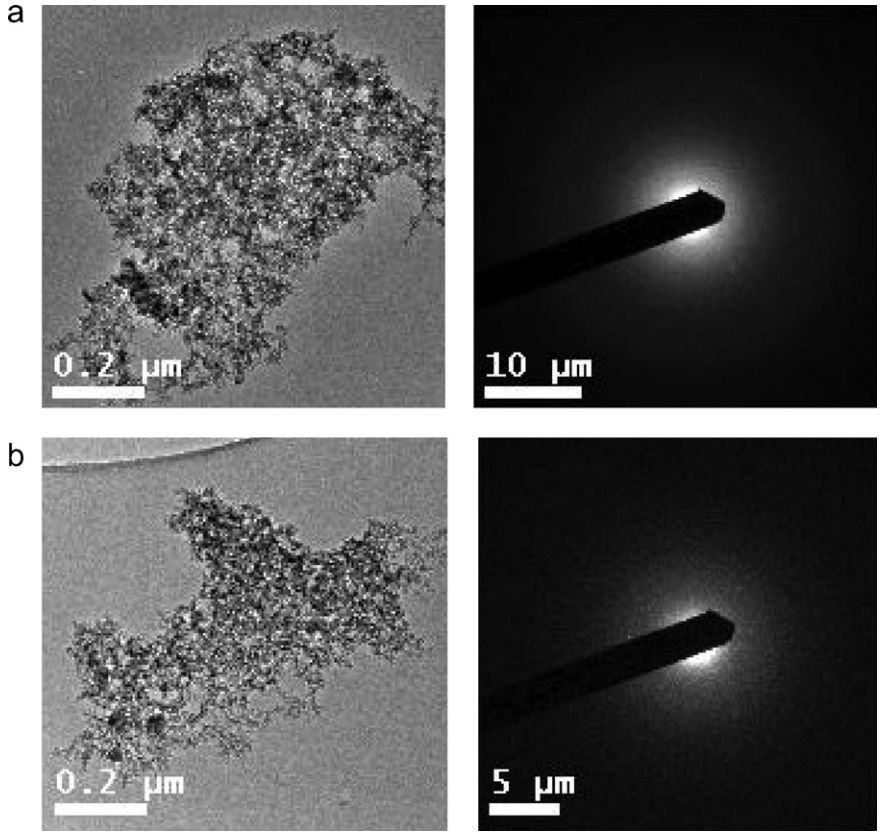

Fig. 4. TEM image and electron diffraction of soot deposited from benzene (a) and benzene–acetonitrile mixture (b).

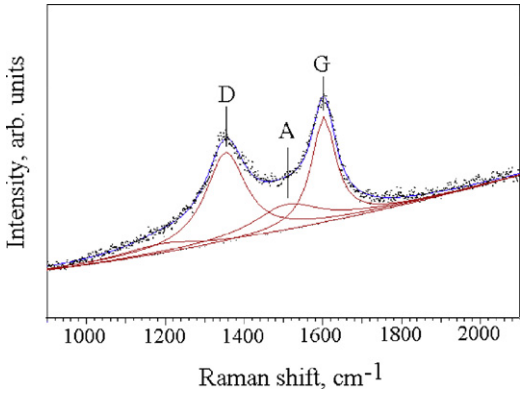

Fig. 5. Raman spectrum of the soot deposited from benzene–acetonitrile mixture.

CH_2CN, CH_3, H, CH_2, CN and C_2H_5 [21,22] and which give rise to shock-tube formation of detected methane and hydrogen cyanide (main products), cyanogen and H_nC_2–CN (n = 1, 3, 5) compounds. Our observation of larger CN-substituted products (the four carbon molecules and benzonitrile) is in line with combination of CH_2CN and CN radicals with C_n/H_m fragments of photolyzed benzene or addition of HCN to C_2H_2. The presence of ethynylbenzene proves the combination of CN and phenyl radicals and suggests, similarly as that of ethynylbenzene in the benzene photolysis, that phenyl radical is a source of cyclic carbonaceous structures.

3.2. Properties of soot

The deposited black soot is difficult to handle, since it keeps electrostatic charge and flows in air. It has large surface area. The determined Brunauer–Emmett–Teller (BET) surface area of the soot deposited from benzene and benzene–acetonitrile mixtures is 176 and 170 m^2/g, respectively. These values indicate similarity of both samples to carbon nanocomposites prepared by MW laser photolysis of toluene and pyridine [15,23].

3.2.1. Electron microscopy

The SEM images of both powders show fluffy morphology (Fig. 3). The SEM-EDX-derived stoichiometries – $C_{1.00}O_{0.08}Si_{0.03}$ (photolysis of benzene) and $C_{1.00}O_{0.12}Si_{0.04}N_{0.05}$ (photolysis of benzene–acetonitrile mixture) – indicate a small incorporation of a silica (silica spallation [15]) and a low content of N element. The incorporation of N confirms reactivity of CN-substituted intermediates produced from benzene–acetonitrile and their inclusion into carbonizing soot.

The TEM images and electron diffraction reveal that both soot samples are amorphous and consist of ca. 10 nm-sized bodies that merge into spongy network (Fig. 4).

3.2.2. Raman spectra

The visible Raman spectra of both soot samples show broad bands at 1350–1365 cm^{-1} (D-band) and 1575–1600 cm^{-1} (G-band) of unsaturated sp^2 carbon with intensity ratio I_D/I_G = 0.50–0.60. Typical spectrum of the sample obtained from benzene–acetonitrile mixture is illustrated on Fig. 5. The G-band reflects stretches of all pairs of sp^2 atoms in rings and chains, the D-band relates to breathing modes of rings [24,25]. The shoulder of the G-band becomes more apparent upon deconvolution of the G-band and corresponds to a contribution of amorphous carbon (A-band) [26] which is peaked at 1510–1530 cm^{-1}. The identified D, G and A bands and the I_D/I_G values are consistent with a disordered graphitic carbon. The observed high photoluminescence background is suggestive of a contribution of a polymeric component, since similar photoluminescence was also observed [27] in a-C:H carbon

3.2.3. XPS spectra

The XPS spectral analysis-derived stoichiometry of superficial layers of both soot samples – $C_{1.00}Si_{0.07}O_{0.15}$ (photolysis of benzene) and $C_{1.00}Si_{0.04}O_{0.19}N_{0.05}$ (photolysis of benzene–acetonitrile mixture) – shows the prevalence of carbon and low content of Si, O and N elements. The presence of oxygen points out to easy oxidation of topmost layers. Binding energies of C1s, N1s and O1s electrons in both samples are in the given order 284.6, 399.6 and 532.5 eV. The C1s spectra are asymmetric in the region of higher energies and resemble spectrum of glassy carbon. The N1s and O1s spectra respectively correspond to N in nitriles and O in C–OH bonds [28]. An estimation of the sp^3/sp^2 hybridization ratios [29,30] was performed by using the energy difference between the most positive maximum and most negative minimum of the C KLL derivative spectra. These values – 18.0 eV for soot from benzene and 17.2 eV for soot from benzene–acetonitrile mixture – were compared (Fig. 6) to those of diamond (13.1 eV) and graphite (21.9 eV) and found as respectively consistent with 70 and 60% of sp^2 state. We thus assume that both soot samples have very similar carbon structure and that sp^2 state population in the N-containing soot is decreased due to small proportion of C≡N groups.

3.2.4. FTIR spectra

The FTIR spectra of the soot from benzene and benzene–acetonitrile mixture (Fig. 7) have similar absorption pattern consisting of bands of C–H stretches centered at 2920–2840 cm^{-1}, a ν(C=O) band at 1720–1730 cm^{-1}, a broad ν(C=C) band at 1550–1650 cm^{-1} and a ν(C–O) band at 1000–1300 cm^{-1}. Absorption bands at lower wavenumbers correspond to C–H deformation and C–C skeletal vibrations. The three distinct bands of the soot from benzene at 2720, 1455 and 1380 cm^{-1} (as well as similar absorption for the soot from benzene–acetonitrile mixture) correspond to stretches and deformation vibrations of –(O–)C–H moieties found [31] e.g. in aromatic methylene dioxy compounds. The spectrum of the soot from benzene–acetonitrile mixture has, in addition, a band at

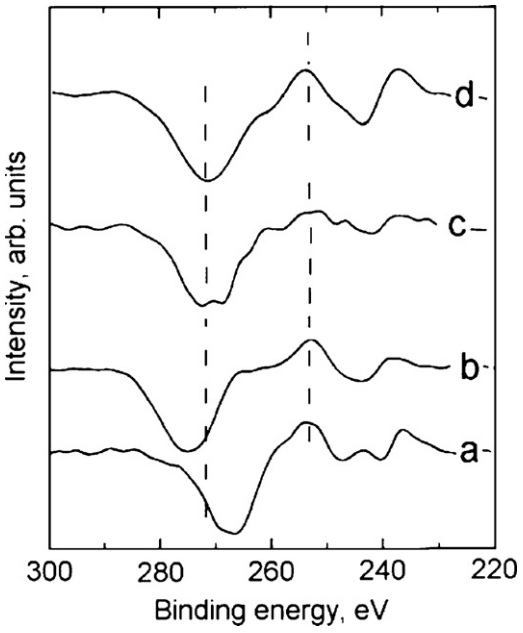

Fig. 6. C KLL X-ray excited derivative Auger spectra of natural diamond (a), grahite (b), and soot obtained with benzene (c) and benzene–acetonitrile mixture (d).

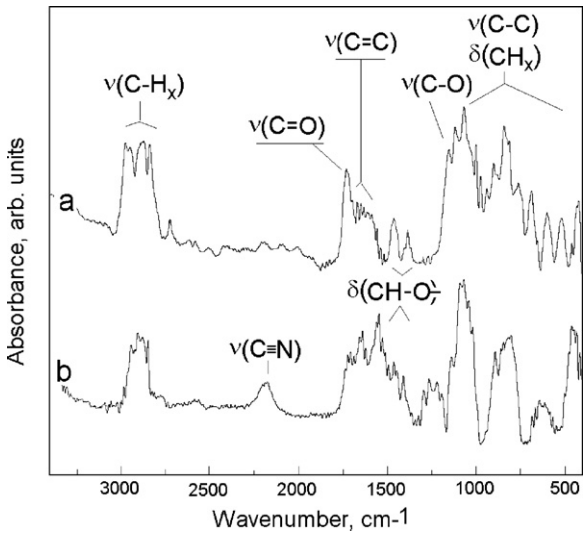

Fig. 7. FTIR spectra of the soot from benzene (a) and benzene–acetonitrile mixture (b).

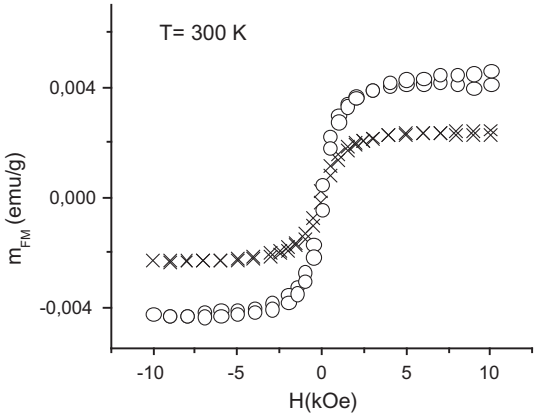

Fig. 8. The hysteresis loops at room temperature for soot obtained from benzene (×) and acetonitrile–benzene mixture (○).

2180 cm^{-1} (assignable to C≡N stretch) and at 1200–1300 cm^{-1} (tentatively assignable to –C=N–O structure).

3.2.5. Magnetic measurements

The magnetic measurements revealed that soot from benzene (B) and acetonitrile–benzene (AB) exhibit, in addition to a small diamagnetic (DM) background, a paramagnetic (PM) and a minor ferromagnetic (FM) contributions. The measured magnetization m can be thus expressed as a sum of 3 terms in the form $m = m_{DM} + m_{PM} + m_{FM}$. The FM magnetization can be evaluated at room temperature (RT), where the PM and DM contribution is proportional to the applied magnetic field H. In Fig. 8, the hysteresis loops m_{FM}(H) measured at room temperature are shown. For both samples the loop exhibits a small coercivity and a finite remanent magnetization. The saturation magnetizations at room temperature m_{FM}(sat) are listed in Table 1. (Let us remark that

Table 1
Magnetic parameters of soot.

Sample from	m_{FM}(sat) (RT) (emu/g)	C (emu K/(g Oe))	m_{PM}(sat) (emu/g)
Benzene	0.00235	3.6×10^{-6}	0.0357
Acetonitrile–benzene	0.0043	7.2×10^{-6}	0.0637

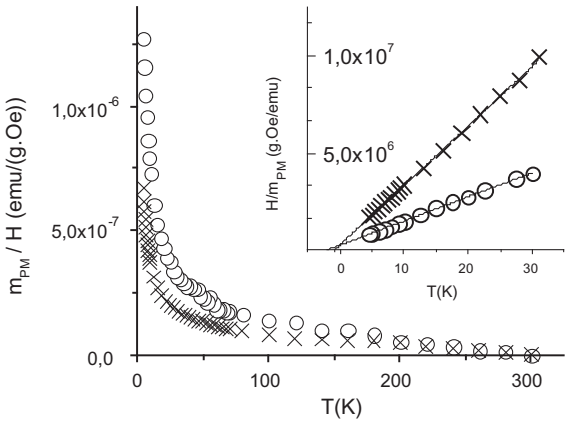

Fig. 9. Temperature dependence of m_{PM}/H for soot obtained from benzene (×) and acetonitrile–benzene mixture (○). In the inset the value H/m_{PM} corresponding to the inverse susceptibility $1/\chi$ and the straight lines extrapolated to $H/M \to 0$.

m_{FM} represents an apparent saturation magnetization related to the total weight of the sample.) The ferromagnetic moment is with highest probability given only by a part of the total volume, where the intrinsic saturation magnetization M_S is much larger (see [32]). Towards lower temperatures m_{FM}(sat) increases and at $T = 10$ K achieves for both samples the value roughly equal 1.5 m_{FM}(sat) (300 K).

The PM magnetization was examined by measuring the temperature dependence of m under an applied field $H = 10$ kOe and field dependence $m(H)$ at $T = 2$ K. The m_{PM} contributions obtained after subtracting $m_{DM} + m_{FM}$ are shown in Figs. 9 and 10. In this procedure the temperature dependence of m_{FM} was assumed to be in the form used e.g. in [15] and field dependence was described by the exponential relation $m = m_0\ (1 - \exp(-\alpha H))$. The temperature dependence $m_{PM}(T)$ was approximated by the Curie–Weiss law $m_{PM} = C/(T - \theta)$, where C is the Curie constant (Table 1) and θ a temperature connected with an exchange interaction between the PM centers. The quality of this approximation in the low temperature region is demonstrated by a straight line character of the $1/\chi$ vs. T plot (inset of Fig. 9). The temperatures θ determined as intercepts on the T axis are −1 and −2.2 K for the B and AB sample respectively, with the accuracy better than 10%. Let us remark that in the whole temperature region, i.e. up to 300 K the quality of the C–W approximation is not so good mainly with respect to an uncertainty in the substracted m_{FM} component. From the

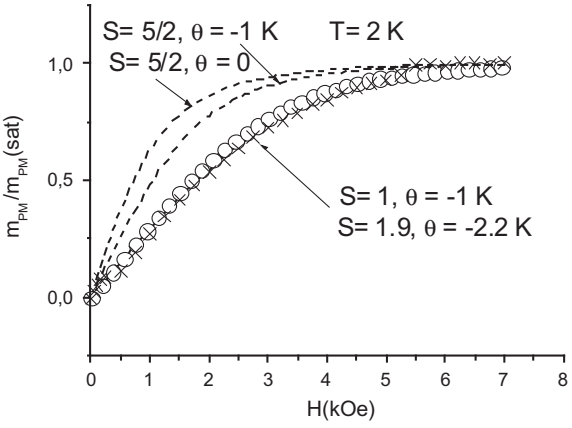

Fig. 10. The reduced PM magnetization vs. magnetic field for soot obtained from benzene (×) and acetonitrile–benzene mixture (○). By the full line the theoretical calculation for $g = 2$, $S = 1$, $\theta = -1$ K and almost identical curve for $g = 2$, $S = 1.9$, $\theta = -2.2$ K, by the dashed lines the calculations for $S = 5/2$ with $\theta = 0$ and −1 K.

field dependence $m_{PM}(H)$ at $T = 2$ K we determined the saturated PM magnetization $m_{PM}(sat)$ by extrapolating m_{PM} $(1/H)$ to the value $1/H = 0$ (Table 1). In Fig. 10 the reduced PM magnetization $m_{PM}/m_{PM}(sat)$ is displayed as a function of H. For a given spin S, g-factor $g = 2$ and temperature θ the reduced magnetization should follow a Brillouin-like function, which can be obtained by solving a transcendental equation with the Brillouin function on the right side. Starting from the values of θ determined above, the best fit for the B and AB soots yields $S = 1$ and $S = 1.9$ respectively. In Fig. 10 we show reduced magnetization fit for the B and AB samples and also for comparison the $S = 5/2$ and $S = 1$ curves for $\theta = 0$.

In the discussion, we first consider the possibility that the observed moment arises from transition metal (typically Fe) impurities for which the content was determined to be less than 20 ppm. In the case of the PM magnetic moment it is necessary to compare the measured saturated PM moment (Table 1) with the estimated saturated PM magnetizations $m_{PMimp}(sat)$ 0.008, 0.008, 0.006, 0.004 emu/g corresponding to 20 ppm of the ions Fe^{3+}, Mn^{2+}, Co^{2+}, Ni^{2+} respectively. We see that for Co^{2+} and Ni^{2+} the measured value is by an order of magnitude larger than $m_{PMimp}(sat)$, which practically excludes a larger influence of Ni^{2+} and Co^{2+} impurities. For Fe^{3+} and Mn^{2+} ions this ratio is about 8 (AB) and 4 (B), but in this case an additional argument can be given suggesting the intrinsic nature of the PM contribution. This is the field dependence of the reduced magnetization (Fig. 10) which seems to correspond to the values of the spins $S = 1$ and $S = 1.9$ in contrast to the course $S = 5/2$ expected for Fe^{3+} and Mn^{2+} impurities. For the FM moment an impurity FM contribution at room temperature can be produced by Fe, Co or Ni atoms. In the same way as for the PM impurities an estimate of $m_{FMimp}(sat)$ leads to 0.004, 0.0033, and 0.001 emu/g for Fe, Co and Ni respectively. The measured value m_{FM} for the AB sample exceeds $m_{FMimp}(sat)(Fe)$ and in the case of the B sample m_{FM} is less than $m_{FMimp}(sat)(Fe)$. Taking into account these facts we may assume that the measured PM and FM magnetizations are unlikely to be caused by impurities, but are predominantly of the intrinsic nature. The PM magnetization $m_{PM}(sat)$ for the B and AB samples are equivalent to 9×10^{-5} and 1.8×10^{-4} μ_B per carbon atom respectively (1 μ_B corresponds to $S = 1/2$). In the same way, for the FM apparent saturation magnetization we obtain 5.9×10^{-6} and 1.2×10^{-5} μ_B per carbon atom. The ratio between the PM and FM magnetizations is for both soot samples nearly the same ($\approx$15), which suggests that the FM moment is caused only by a small part ($\approx$1/15) of the centers which are ferromagnetically exchange coupled. A ferromagnetically active relative volume (or weight) can be very roughly estimated from the ratio m_{FM}/M_s, where the real saturation magnetization $M_s \approx 10$ emu/g [32]. This yields 0.0036 and 0.0064 for the B and AB soot samples respectively. The magnetizations of both samples are very small but we may state a positive influence connected with N doping in the AB sample. For the B sample the PM magnetization seems to be caused by dangled bonds (2 electrons, $S = 1$) and in the AB case there exist probably paramagnetic centers formed by pairs of the dangled bonds (4 electrons, $S = 2$).

We note that carbon magnetism [33] was observed in various carbon materials as e.g. highly oriented pyrolytic graphite [34], pyrolytic carbons [35,36], N-containing carbons [37], chemically modified [38], laser ablatively [39] and plasma chemical vapor deposited [40] carbon and in carbon nanostructures (e.g. laser-ablatively prepared nanofoam [41], ion-implanted nanodiamond from detonation process [42], hydrogenated carbon nanotubes [43] or laser chemical vapor deposited carbon/polyoxocarbosilane nanocomposite [15]). However, some results were not checked for impurities or later reproduced [35,36,38] and indicated only paramagnetism [39] and the absence of magnetic order in amorphous carbon [39,41].

This phenomenon of carbon magnetism is of continuing interest (e.g. [32,33,34,44,45]), but it is still not well understood. Our data are in qualitative agreement with the occurrence of ferromagnetic and paramagnetic spins located on C (and also possibly on N [37]) atoms. A contribution from dangling Si-bonds of the minor diamagnetic SiO_2 constituent can be ruled out.

3.2.6. Possible chemical modification

We note that the incorporation of –CN group into the carbonaceous network keeps a promise for synthesis of other nanobodies, because the –CN group can be changed for other substituents through nucleophilic addition, reduction or hydrolysis. Such chemical modification of nanosoot has been previously described for Cl-substituted nanosoot [46] that was found reactive with nucleophilic ammonia.

4. Conclusions

KrF laser photolysis of benzene yields low amounts of unsaturated hydrocarbons and allows chemical vapor deposition of amorphous ultrafine soot. These products are compatible with carbonization of benzene.

The photolysis of benzene in the presence of non-absorbing acetonitrile yields the same unsaturated hydrocarbons together with HCN, cyanogens and a number of volatile CN-substituted hydrocarbons and allows deposition of amorphous ultrafine CN-substituted soot. These products are compatible with decomposition of acetonitrile in sooting benzene and with incorporation of CN-substituents in the forming carbonaceous phase.

The respective solid materials have large surface area and were identified as ca.10 nm-sized bodies agglomerated into spongy agglomerates. They contain C–H bonds, have a structure of disordered graphite and their sp^3/sp^2 hybridization ratios consistent with 70 and 60% of sp^2 state. Both soot samples are reactive to atmosphere and develop C=O bonds. They belong among carbon magnets and show both paramagnetic and ferromagnetic contributions.

We suggest that CN-containing soot may be chemically modified through reactions on the CN bonds and similarly as Cl-substituted nanosoot [46] could find use as a precursor for construction of novel nanobodies.

Acknowledgement

This work was supported by GA ASCR (Grant 400720619).

References

[1] J.K. Foote, M.H. Mallon, J.N. Pitts, The vapour phase photolysis of benzene at 1849 A, J. Am. Chem. Soc. 88 (1966) 3698–3702, and references therein.
[2] F. Mellows, S. Lipsky, Hydrogen atom yield from benzene photolyzed at 1849 A, J. Phys. Chem. 70 (1966) 4076–4077.
[3] L. Kaplan, S.P. Walch, K.E. Wilzbach, Photolysis of benzene vapor at 1849 A formation of cis-1,3-hexadien-5-yne, J. Am. Chem. Soc. 90 (1968) 5646–5647.
[4] A. Yokoyama, X. Zhao, E.J. Hintsa, R.E. Continetti, Y.T. Lee, Molecular beam studies of the photodissociation of benzene at 193 and 248 nm, J. Chem. Phys. 92 (1990) 4222–4234.
[5] S.-T. Tsai, C.-K. Lin, Y.T. Lee, C.-K. Ni, Dissociation rate of hot benzene, J. Chem. Phys. 113 (2000) 67–71.
[6] S.-T. Tsai, C.-L. Huang, Y.T. Lee, C.-K. Ni, Ring opening dissociation of D6-benzene, J. Chem. Phys. 115 (2001) 2449–2456.
[7] V.V. Kislov, T.L. Nguyen, A.M. Mebel, S.H. Lin, S.C. Smith, Photodissociation of benzene under collision-free conditions: an ab initio Rice–Ramsperger, Kassel–Marcus study, J. Chem. Phys. 120 (2004) 7008–7017, and references therein.
[8] Y Honjo, T. Kinoshita, T. Yatsuhashi, N. Nakashima, Formation of 1,3-hexadiene-5-yne by two-photon chemistry of benzene via hot molecule, J. Photochem. Photobiol. A: Chem. 171 (2005) 223–229.
[9] W.M. Hetherington III, G.M. Korenowski, K.B. Eisenthal, Picosecond cars as a probe of the multiphoton photofragmentation of benzene, Chem. Phys. Lett. 77 (1981) 275–279.

[10] L. Zandee, R.B. Bernstein, Resonance-enhanced multiphoton ionization and fragmentation of molecular beams: NO, I_2, benzene, and butadiene, J. Chem. Phys. 71 (1979) 1359–1372.
[11] Y. Mori, Y. Kitagawa, Multiphoton ionization and fragmentation process of benzene at 193 nm involving ionization of neutral fragments, Bull. Chem. Soc. Jpn. 66 (1993) 1043–1052.
[12] J.P. Reilly, K.L. Kompa, Laser induced multiphoton ionization mass spectrum of benzene, J. Chem. Phys. 73 (1980) 5468–5477.
[13] N. Nakashima, H. Inoue, M. Sumitani, K. Yoshihara, Laser flash photolysis of benzene. II. Laser-induced cluster formation in gas phase, J. Chem. Phys. 73 (1980) 4693–4694.
[14] M. Kauer, H.G. Wagner, Photocondensation in benzene vapor using a single-pulse UV laser, Z. Phys. Chem. 153 (1987) 109–127.
[15] J. Pola, S. Bakardjieva, M. Maryško, V. Vorlíček, J. Šubrt, Z. Bastl, A. Galíková, A. Ouchi, Laser-induced conversion of silica into nanosized carbon–polyoxocarbosilane composites, J. Phys. Chem. C 111 (2007) 16818–16826.
[16] J.H. Kiefer, L.J. Mizerka, M.R. Patel, H.-C. Wei, A shock tube investigation of major pathways in the high temperature pyrolysis of benzene, J. Phys. Chem. 89 (1985) 2013–2019.
[17] H.F. Calcote, Mechanism of soot nucleation in flames – a critical review, Combust. Flame 42 (1981) 215–242.
[18] S.-I. Shih, T.-C. Lin, M. Shih, Decomposition of benzene in the RF plasma environment. Part II. Formation of polycyclic aromatic hydrocarbons, J. Hazard. Mater. B 117 (2005) 149–159.
[19] R.F.C. Brown, Pyrolytic Methods in Organic Chemistry, Organic Chemistry Monographs, vol. 41, Academic Press, New York, 1980.
[20] F. Stahl, P.R.v. Schleyer, H.F. Schaefer III, R.I. Kaiser, Reactions of ethynyl radicals as a source of C_4 and C_5 hydrocarbons in Titan's atmosphere, Planet Space Sci. 50 (2002) 685–692.
[21] A. Lifshitz, A. Moran, S. Bidani, Thermal reactions of acetonitrile at high temperatures. Pyrolysis behind reflected shocks, Int. J. Chem. Kinet. 19 (1987) 61–79.
[22] A. Lifshitz, C. Tamburu, Thermal decomposition of acetonitrile. Kinetic modeling, Int. J. Chem. Kinet. 30 (1998) 341–347.
[23] J. Pola, A. Ouchi, S. Bakardjieva, V. Vorlíček, M. Maryško, J. Šubrt, Z. Bastl, Laser photochemical etching of silica: nanodomains of crystalline chaoite and silica in amorphous C/Si/O/N phase, J. Phys. Chem. C 112 (2008) 13281–13286.
[24] R.O. Dillon, J.A. Woollam, V. Katkanant, Use of Raman scattering to investigate disorder and crystalline formation in as-deposited and annealed carbon films, Phys. Rev. B 29 (1984) 3482–3489.
[25] A.C. Ferrari, J. Robertson, Interpretation of Raman spectra of disordered and amorphous carbon, Phys. Rev. B 61 (2000) 14095–14107.
[26] R.N. Tarrant, D.R. McKenzie, M.M.M. Bilek, Raman characterization of PIII multilayer carbon films, Diamond Relat. Mater. 13 (2004) 1422–1426.
[27] C. Casiraghi, A.C. Ferrari, J. Robertson, Raman spectroscopy of hydrogenated amorphous carbons, J. Phys. Rev. B 72 (085401) (2005) 14 p.
[28] NIST X-ray Photoelectron Spectroscopy Database 20, Version 3.5 (2030; http://srdata.nist.gov/xps/.
[29] A.A. Galuska, H.H. Madden, R.E. Allred, Electron spectroscopy of graphite, graphite oxide and amorphous carbon, Appl. Surf. Sci. 32 (1988) 253–272.
[30] J.C. Lascovich, R. Giorgi, S. Scaglione, Evaluation of the sp^2/sp^3 ratio in amorphous carbon structure by XPS and XAES, Appl. Surf. Sci. 47 (1991) 17–21.
[31] R.G.J. Miller, H.A. Willis, Infrared Structural Correlation Tables, Spectrum House, Heyden & Son, Ltd., London, 1969.
[32] H. Ohldag, P. Esquinazi, E. Arenholz, D. Spemann, M. Rothermel, E. Setzer, T. Butz, The role of hydrogen in room-temperature ferromagnetism at graphite surfaces, New J. Phys. 12 (2010) 123012 (10 p).
[33] T.L. Makarova, Studies of High-Temperature Superconductivity, Nova Science Publisher, Inc., New York, 2003.
[34] P. Esquinazi, A. Setzer, R. Höhne, C. Semmelhack, Y. Kopelevich, D. Spemann, T. Butz, B. Kohlstrunk, M. Lösche, Ferromagnetism in oriented graphite samples, Phys. Rev. B 66 (2002) 024429 (10 p).
[35] A.A. Ovchinnikov, V.N. Spector, Organic ferromagnets, new results, Synth. Metals 27B (1988) 615–624.
[36] K. Murata, H. Ushijima, H. Ueda, K. Kawaguchi, A stable carbon-based organic magnet, J. Chem. Soc. Chem. Commun. (1992) 567–569.
[37] H. Araki, K. Toshibo, Spontaneous magnetization phenomena in pyrolyzed organic compounds containing nitrogen atoms, Jpn. J. Appl. Phys. 31 (1992) L130–L133.
[38] H. Pardo, R. Faccio, F.M. Araújo-Moreira, O.F. de Lima, A.W. Mombrú, Synthesis and characterization of stable room temperature bulk ferromagnetic graphite, Carbon 44 (2006) 565–569.
[39] R. Höhne, K.-H. Han, P. Esquinazi, A. Setzer, H. Semmelhack, D. Spemann, T. Butz, Magnetism of pure, disordered carbon films prepared by pulsed laser deposition, J. Magn. Magn. Mater. 272–276 (2004) e839–e840.
[40] T. Saito, T. Ozeki, K. Terasníma, Magnetism in diamond-like carbon, Solid State Commun. 136 (2005) 546–549.
[41] A.V. Rode, E.G. Gamaly, A.G. Christy, J.G. Fitz Gerald, S.T. Hyde, R.G. Elliman, B. Luther-Davies, A.I. Center, J. Androulakis, J. Giapintzakis, Unconventional magnetism in all-carbon nanofoam, Phys. Rev. B 70 (2004) 054407 (9 p).
[42] S. Talapatra, P.G. Ganesan, T. Kim, R. Vajtai, M. Huang, M. Shima, G. Ramanath, S. Sestava, S.C. Deevi, P.M. Ajayan, Irradiation-induced magnetism in carbon nanostructures, Phys. Rev. Lett. 95 (2005) 097201 (4 p).
[43] A.L. Friedman, H. Chun, Y.J. Jung, D. Heiman, E.R. Glaser, L. Menon, Possible room-temperature ferromagnetism in hydrogenated carbon nanotubes, Phys. Rev. B 81 (2010) 115461 (4 p).
[44] X. Yang, H. Xia, X. Qin, W. Li, Y. Dai, X. Liu, M. Zhao, Y. Xia, S. Yan, B. Wang, Correlation between the vacancy defects and ferromagnetism in graphite, Carbon 47 (2009) 1399–1406.
[45] P. Esquinazi, R. Höhne, Magnetism in carbon structures, J. Magn. Magn. Mater. 290–291 (2005) 20–27.
[46] J. Pola, A. Galíková, S. Bakardjieva, J. Šubrt, Z. Bastl, V. Vorlíček, M. Maryško, A. Ouchi, MW UV laser photolysis of dichloroethene for gas-phase deposition of nanosized chlorinated soot, J. Phys. Chem. C 114 (2010) 16153–16159.